Title

Parallel particle swarm optimization and finite-difference time-domain (PSO/FDTD) algorithm for multiband and wide-band patch antenna designs

Journal

IEEE Transactions on Antennas and Propagation, 53(11)

ISSN

0018-926X

Authors

Jin, N B
Rahmat-Samii, Y

Publication Date

2005-11-01

Peer reviewed

Parallel Particle Swarm Optimization and Finite-Difference Time-Domain (PSO/FDTD) Algorithm for Multiband and Wide-Band Patch Antenna Designs

Nanbo Jin, *Student Member, IEEE,* and Yahya Rahmat-Samii, *Fellow, IEEE*

***Abstract*—This paper presents a novel evolutionary optimization methodology for multiband and wide-band patch antenna designs. The particle swarm optimization (PSO) and the finite-difference time-domain (FDTD) are combined to achieve the optimum antenna satisfying a certain design criterion. The antenna geometric parameters are extracted to be optimized by PSO, and a fitness function is evaluated by FDTD simulations to represent the performance of each candidate design. The optimization process is implemented on parallel clusters to reduce the computational time introduced by full-wave analysis. Two examples are investigated in the paper: first, the design of rectangular patch antennas is presented as a test of the parallel PSO/FDTD algorithm. The optimizer is then applied to design E-shaped patch antennas. It is observed that by using different fitness functions, both dual-frequency and wide-band antennas with desired performance are obtained by the optimization. The optimized E-shaped patch antennas are analyzed, fabricated, and measured to validate the robustness of the algorithm. The measured less than − 18 dB return loss (for dual-frequency antenna) and 30.5% bandwidth (for wide-band antenna) exhibit the prospect of the parallel PSO/FDTD algorithm in practical patch antenna designs.**

***Index Terms*—Finite-difference time-domain (FDTD), parallel computation, particle swarm optimization, patch antenna.**

I. Introduction

PATCH antennas are extensively utilized in wireless communication systems by exploiting their low-profile feature and the ease in fabrication. With recent advances in electromagnetics computer-aided design (CAD), the patch antenna design has benefited from the utilization of accurate numerical methods. Usually the basic antenna topology can be conjectured according to the desired antenna performance. The challenge is to determine the geometric parameters of the antenna, such as the patch dimensions and the feed position, to achieve the best design that satisfies a certain criterion. Many efforts have been expanded on the parametric study of various patch antennas [1]. However, these studies are not systematic and the conclusions are highly dependent on the antenna under investigation. Consequently, a *trial-and-error* process is inevitable in most patch antenna designs.

Recently the particle swarm optimization (PSO) was introduced to the EM community [2] to accommodate this challenge. The initial PSO concept was developed in 1995 [3] as a novel evolutionary optimization (EO) methodology over a complex solution space. Motivated by a social-psychological metaphor, the optimizer applies the information exchange scheme between the individuals in a swarm (i.e., a swarm of bees, a flock of birds or a school of fish) during their food-searching activities. The trajectory of each individual is influenced by its own successful experiences, as well as the successes of its neighbors. As formulated in [2], PSO starts by designating each position in the solution space as a potential design. A fitness function is then defined to quantify the performance of each candidate design. All the encountered positions are evaluated by this fitness function to represent how well the design criterion is satisfied. Finally, toward the end of the optimization, most particles converge to the global optimum, which expectedly results into the best design. Compared to conventional EO algorithms such as the genetic algorithm (GA) [4], PSO takes the advantage of its algorithmic simplicity and robustness. PSO has been applied to many EM applications, such as the one-dimensional (1-D) and 2-D array synthesize [5]–[7], the corrugated horn design [8], and the reflector shaping [9]. The multiobjective optimizations [7], [10], [11] further enhance the performance of PSO by exploiting its inherit versatility and using multiple fitness functions.

This paper presents the application of PSO in multiband and wide-band patch antenna designs. Based on a predetermined antenna topology, the geometrical parameters are extracted and optimized by PSO. The FDTD is combined with PSO kernel to evaluate the fitness functions. The optimization process is implemented on parallel clusters. The feasibility of the parallel PSO/FDTD algorithm allows improved optimization efficiency, higher simulation accuracy, and less computational time. First, it is noticed that the particle positions in PSO are denoted by continuously valued vectors. Knowing a basic antenna structure, the geometrical parameters can be directly optimized without being mapped from decimal to binary. In contrast, in the GA/MOM optimization for patch antennas [12], [13], each candidate design is discretized into pixels and represented by a binary string. The optimal design has to be explored in a larger solution space without applying the *a priori* knowledge. Second, the FDTD provides more accurate fitness evaluations than analytical approximations [14], [15] or spectral-domain methods [12], [13] in multiband and wide-band antenna optimizations. For instance, the antenna return loss can be calculated in the entire frequency domain via a single FDTD simulation, whereas the spectral-domain methods only calculate the antenna's performance at distinct frequencies. Finally, by applying the inherit parallelism of PSO, parallel clusters

Manuscript received November 23, 2004.

The authors are with the Department of Electrical Engineering, University of California, Los Angeles, CA 90095 USA (e-mail: jnnb@ee.ucla.edu; rahmat@ee.ucla.edu).

Digital Object Identifier 10.1109/TAP.2005.858842

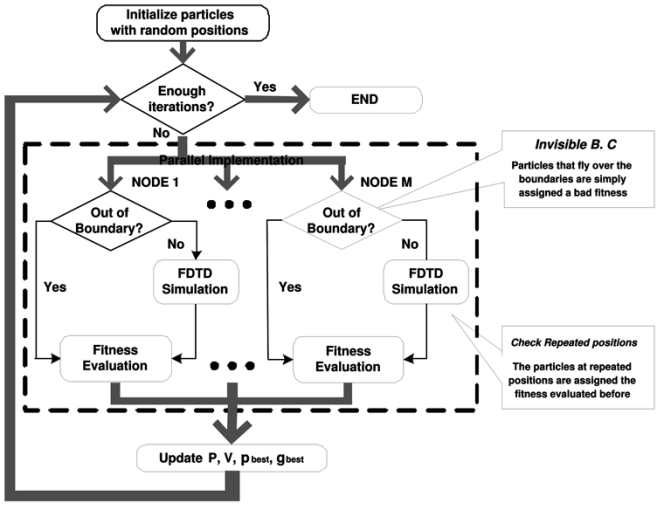

Fig. 1. Flowchart of the parallel PSO/FDTD algorithm. The PSO kernel and PSO/FDTD interface are constructed to prevent physically invalid structures and redundant fitness evaluations. The activities confined by the dashed line are implemented on parallel clusters.

can be utilized to significantly reduce the computational time introduced by full-wave analysis.

Section II details the architecture of the parallel PSO/FDTD algorithm. Section III utilizes the optimization of rectangular patch antennas to illustrate the parallel PSO/FDTD concept. In Section IV, the algorithm is applied to E-shaped patch antenna designs, which represent the optimizations in a 6-D solution space. Using different fitness functions, both dual-frequency and wide-band E-shaped antennas are obtained. Further analysis and simulations of the optimized antennas are presented in this section. The optimized E-shaped antennas are fabricated and measured to validate the applicability of the algorithm in practical patch antenna designs. The paper is summarized in Section V.

II. Parallel PSO/FDTD Algorithm Architecture

The UCLA-PSO algorithm has been tested to be numerically accurate and efficient [2], [11]. With respect to the PSO kernel, the fitness functions are evaluated externally. This enables various EM simulation tools (i.e., FDTD, MoM, PO/PTD) to be utilized as the fitness evaluator without changing the PSO kernel. Fig. 1 shows a flowchart of the parallel PSO/FDTD algorithm. As aforementioned, for each design criterion, the basic antenna structure can be determined *a priori* according to the designer's experience. The geometric parameters of the antenna are extracted to be optimized by the PSO kernel. The position of each particle is determined by these parameters and mapped into a candidate design. The FDTD configuration file is generated by the PSO/FDTD interface. According to the FDTD simulation results, the fitness function is evaluated to represent the performance of the candidate design. The PSO kernel and PSO/FDTD interface are constructed to prevent physically invalid structures and redundant fitness evaluations. The activities confined by the dashed line in Fig. 1 are implemented on parallel clusters.

A. The PSO Kernel

A PSO optimization is initiated by randomly allocating particle positions in the solution space. Assume there are M particles in a swarm, along with N geometrical parameters to be optimized (N is denoted as the dimension of the solution space). The particles' positions and velocities are stored in two $M \times N$ matrices, $\mathbf{X}$ and $\mathbf{V}$, respectively. At each iteration, the velocities of each particle is determined by the distances from its current position to two important locations, which are denoted by the "personal best" ($p_{\rm best}$) and the "global best" ($g_{\rm best}$). The $p_{\rm best}$ is the location where each particle attains its best fitness value up to the present iteration. On the other hand, the $g_{\rm best}$, which is chosen from the M $p_{\rm best}$s, represents the location where the best fitness value was attained by any particle. At each iteration the particles' velocities are calculated according to

$$\mathbf{V}_t = w\mathbf{V}_{t-1} + c_1\eta_1(\mathbf{P}_{t-1} - \mathbf{X}_{t-1})\Delta t + c_2\eta_2(\mathbf{G}_{t-1} - \mathbf{X}_{t-1})\Delta t \quad (1)$$

and the particle's positions are updated by

$$\mathbf{X}_t = \mathbf{X}_{t-1} + \mathbf{V}_t\Delta t. \quad (2)$$

In the equations above, t denotes the current iteration, and Δt is the time interval between two consecutive iterations which is assumed to be unity. $\mathbf{P}$ and $\mathbf{G}$ are $M \times N$ matrices where the $p_{\rm best}$s and the $g_{\rm best}$ are refreshed and stored at each iteration. All the M rows of $\mathbf{G}$ are identical since all the particles have the same $g_{\rm best}$.

Equations (1) and (2) show explicitly that a particle always apply its own and other particles' successes as the strategy to adjust its trajectory. In (1), a time-varying coefficient w, which is called *inertial weight* [16], decreases linearly from a maximum w_1 when the optimization starts to a minimum w_2 toward the end. It has the effect of changing the scale of exploration from global to localized during the entire course. In this paper, the best trade-off between the particle convergence and a fully searched solution space is obtained by using $(w_1, w_2) = (0.9, 0.4)$. Two random variables, η_1 and η_2, are both uniformly distributed within [0, 1] to inject the unpridictablility in the swarm behavior. The constant coefficients $c_1 = c_2 = 2.0$ are multiplied to adjust the "nostalgia" and the social influence between the particles.

In a PSO optimization, the particles that fly out of the solution space must be properly handled. The out-of-boundary particles usually lead to physically invalid designs, therefore an error will be encountered by the fitness evaluator and the recursive optimization process will be corrupted. In this paper, the *invisible* boundary condition [2] is used in the parallel PSO/FDTD algorithm. Unlike other boundary conditions such as *absorbing walls* and *reflecting walls*, the *invisible* boundary condition allows the particles to fly over the boundary of the solution space. These out-of-boundary particles are simply assigned a very bad fitness value. Since only the particles currently located in the solution space will be evaluated by the FDTD algorithm, the number of overall fitness evaluations is reduced. It should be noted that the out-of-boundary particles are not abandoned but

still communicate with their counterparts. They will be evaluated in later iterations after coming back to the solution space. The total number of particles at each iteration is fixed during the optimization.

B. The PSO/FDTD Interface for an Efficient Optimization

In the PSO/FDTD algorithm, an interface is constructed between PSO and FDTD executable files for necessary data transmissions and extractions. At the beginning of each iteration, the PSO/FDTD interface is called after the PSO kernel writes the particle positions using the information achieved from the last iteration. The interface then reads each particle's position, maps it into a candidate design and generates a configuration file for the FDTD simulation. After the candidate design being simulated, the interface is called again to extract the desired antenna performance and evaluate the fitness function. The current iteration ends by transmitting the fitness values back to the PSO kernel to calculate the particle positions in the next iteration.

Due to the computational cost introduced by FDTD, the fitness evaluation is the most time-consuming part in an optimization. Therefore, it is critical to reduce the unnecessary fitness evaluations to achieve an efficient optimization. The *invisible* boundary condition implemented in the PSO kernel mitigates the need to simulate the out-of-boundary particles; however, nothing is more efficient in eliminating the redundant fitness evaluations than applying the *repeated position checking* (RPC) scheme in the PSO/FDTD interface.

The redundant simulations are introduced when mapping a particle position into a candidate design. Here the continuously valued particle position (which denotes the antenna geometrical parameters) has to be discertized in the FDTD configuration file. This arises a possibility that different particle positions are mapped into the same candidate design. To illustrate this fact, we assume that x_i is the i^{th} component of a N-dimensional particle position vector, $\vec{x}$. We also assume the grid size in FDTD algorithm is Δd. All the particle positions located in

$$x_i \in \left[\Delta dm_i - \frac{\Delta d}{2},\ \Delta dm_i + \frac{\Delta d}{2}\right) \qquad i = 0, 1, 2\cdots, N.\ m_i\text{s are integers.} \quad (3)$$

are defined as *repeated positions* with respect to the vector $[m_1,\ m_2, \ldots, m_N]$. This is because all these positions result in the same FDTD output as that when

$$\vec{x} = [\Delta dm_1,\ \Delta dm_2, \ldots, \Delta dm_N], \qquad m_i\text{s are integers} \quad (4)$$

is used as the input of FDTD algorithm.

The RPC scheme generates an archive to record the fitness values of all *not-repeated positions*. This archive is updated at each iteration. All the particle positions are compared to this archive before being mapped: the *repeated positions* are directly assigned their associated fitness values that are calculated in previous iterations and stored in the archive. Only the *not-repeated positions* are simulated by FDTD, with their fitness values added to the archive afterward. This search-compare process takes time; however, it is negligible compared to the time cost of a FDTD simulation. The effect of applying the RPC scheme in reducing the optimization time cost will be presented in later sections.

C. Parallel PSO/FDTD Implementation

The optimization process is implemented on parallel clusters to further reduce the computational time. PSO is parallel by nature since each particle can be regarded as an independent agent. Parallel computation benefits the algorithm by providing each agent with one of the parallel processors. Compared to the computational time in fitness evaluations, the calculation of particle positions and velocities is just a small fraction of the entire course. The master-slave approach [17] is hence practical to construct the parallel PSO architecture. With only one master node tracking the particles and collecting simulation results, the particles are distributed to a bunch of slave nodes to perform FDTD fitness evaluations. Identical FDTD code is stored on each slave node with PSO executable files. The particle positions and velocities are transmitted from the master node, and the FDTD configuration files are generated on the slave nodes by PSO/FDTD interface.

The master-slave system was constructed on the UCLA Advanced Technology Service's Beowulf Linux cluster. The system has 64 batch process nodes, each with two Intel Xeon 3.0-GHz processors and 2-GB RAM. The Message Passing Interface (MPI) was used to communicate between the master and slave nodes. Theoretically there should be as many slave nodes as the number of particles; however, due to the limitation in the system's availability, most optimizations in this paper utilizes 4 parallel processors for a 10-particle swarm.

III. A Test of the Parallel PSO/FDTD Algorithm: Rectangular Patch Antenna Designs

As a test of the parallel PSO/FDTD algorithm, the optimizer is applied to a basic antenna design problem in this section. It is desired to design a rectangular patch antenna that satisfies some specific requirements on its resonant frequency and bandwidth. The antenna performance is investigated near a desired frequency of 3.1 GHz. The three geometrical parameters to be optimized are the patch length L, the patch width W and the feed position x, as shown in Fig. 2. The ground plane is fixed at 60 mm $\times$ 60 mm. A 3-mm-thick dielectric with $\varepsilon_r = 2.2$ is used as the substrate. The grid size in the FDTD simulation is 1 mm, in order to achieve both reasonable simulation time and acceptable accuracy.

The geometrical parameters are optimized within (unit: mm)

$$L \in (0, 44); \quad W \in (0, 44); \quad x \in (0, 22) \quad (5)$$

Neither L nor W exceeds $0.75W_g$ (W_g is the dimension of the ground plane) to maintain a good front-to-back ratio in the radiation pattern. On the other hand, the feed can not go beyond the patch since it generates a physically invalid structure. An additional geometrical restriction of

$$x < \frac{L}{2} \quad (6)$$

should be also satisfied. Equations (5) and (6) completely define the boundary of the solution space.

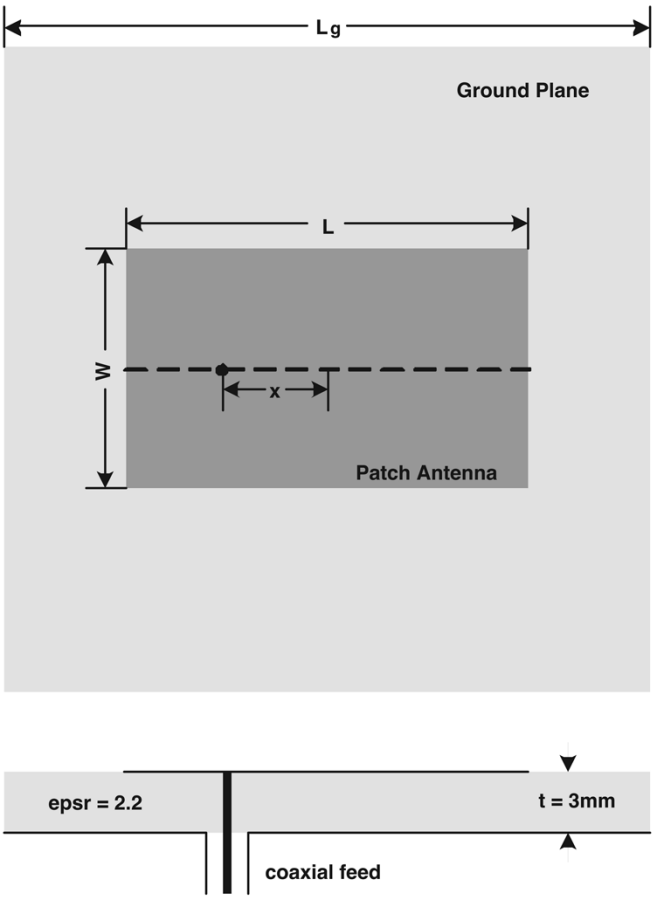

Fig. 2. Configuration of a coaxial-fed, rectangular patch antenna. The length L, width W, and feed position x of the patch need to be optimized. A 3-mm-thick substrate with $\varepsilon_r = 2.2$ and a 60 mm × 60 mm ground plane are fixed in the optimization.

The selection of the particle number and the maximum iteration depends on the dimension of the solution space and the fitness function. Our experimental result based on standard PSO testing fitness functions (i.e., 10-D Rosenbrock function, etc.) shows that, the number of particles should be comparable to the dimension of the solution space to obtain a good convergence. A reasonably large number of iterations are also necessary for the particles to get converged. In this rectangular patch antenna design, a 10-particle-swarm and a maximum of 200 iterations are utilized.

To fully test the performance of the optimizer using different fitness functions, two rectangular patch antennas satisfying different design criteria are optimized: 1) Antenna I has the best return loss at $f_r = 3.1$ GHz; 2) Antenna II has the best bandwidth ($S_{11} < -10$ dB) around $f_r = 3.1$ GHz. Two independent optimizations are set up with the same swarm configuration, the same solution space but different fitness functions. In the PSO kernel, a better design is defined to have a lower fitness value, therefore the fitness functions are defined as

$$f_1 = 50 + S_{11,\,\text{at 3.1 GHz}}, \quad \text{for antenna I} \tag{7}$$

and

$$f_2 = (50 + S_{11,\text{at 3.1 GHz}}) + (50 - 500 \times BW) \quad \text{for antenna II.} \tag{8}$$

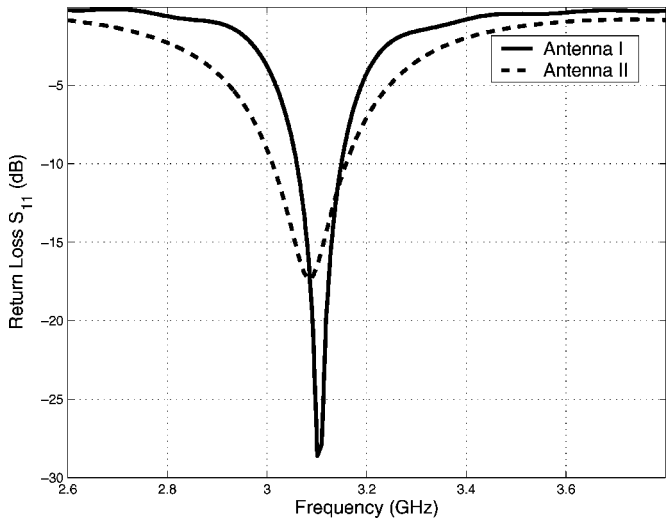

Fig. 3. Simulated S_{11} curves of the two optimized rectangular patch antennas. Both antennas resonate at $f = 3.1$ GHz. Antenna II is observed to have a greater $S_{11} < -10$ dB bandwidth due to the larger patch width.

TABLE I
GEOMETRICAL PARAMETERS OF THE OPTIMIZED RECTANGULAR PATCHES (UNIT: MILLIMETERS)

Design	L	W	x
Antenna I	30.0	18.0	4.0
Antenna II	30.0	44.0	12.0

Here the S_{11} terms are all negative values in dB. A constant of 50 is added to guarantee that the fitness value is positive. The BW term in (8) denotes the $S_{11} < -10$ dB bandwidth in GHz. For most rectangular patch antennas, the fractional bandwidth is only several percentages. The bandwidth term is hence multiplied by a factor of 500 to achieve an appropriate impact to the fitness value. The first term in (8) gives a reward to the antennas resonating at 3.1 GHz, which means our interest is not only a broader bandwidth but also the desired center frequency of the $S_{11} < -10$ dB band.

Fig. 3 shows the simulated S_{11} curves of the optimized antennas. With f_1 only addressed on the resonant frequency, antenna I exhibits an S_{11} of -28 dB at the desired frequency of 3.1 GHz. A bandwidth of 90 MHz (2.9%) is observed. On the other hand, with the bandwidth information incorporated in f_2, antenna II has a deteriorated S_{11} of -17 dB at 3.1 GHz but an increased bandwidth of 150 MHz (4.8%). These results convinced us that different fitness functions can be properly defined to achieve different desired antenna performances.

The geometrical parameters of the optimized rectangular patch antennas are shown in Table I. It is observed that both antennas have the same length of 30.0 mm, while antenna II has a much larger patch width. Reference [18] gives the empirical formulas for rectangular patch antenna design

$$L \approx 0.49 \frac{\lambda_0}{\sqrt{\epsilon_r}} \tag{9}$$

$$BW \approx 3.77 \frac{\epsilon_r - 1}{\epsilon_r^2} \frac{W}{L} \frac{t}{\lambda_0}, \quad \frac{t}{\lambda_0} \ll 1 \tag{10}$$

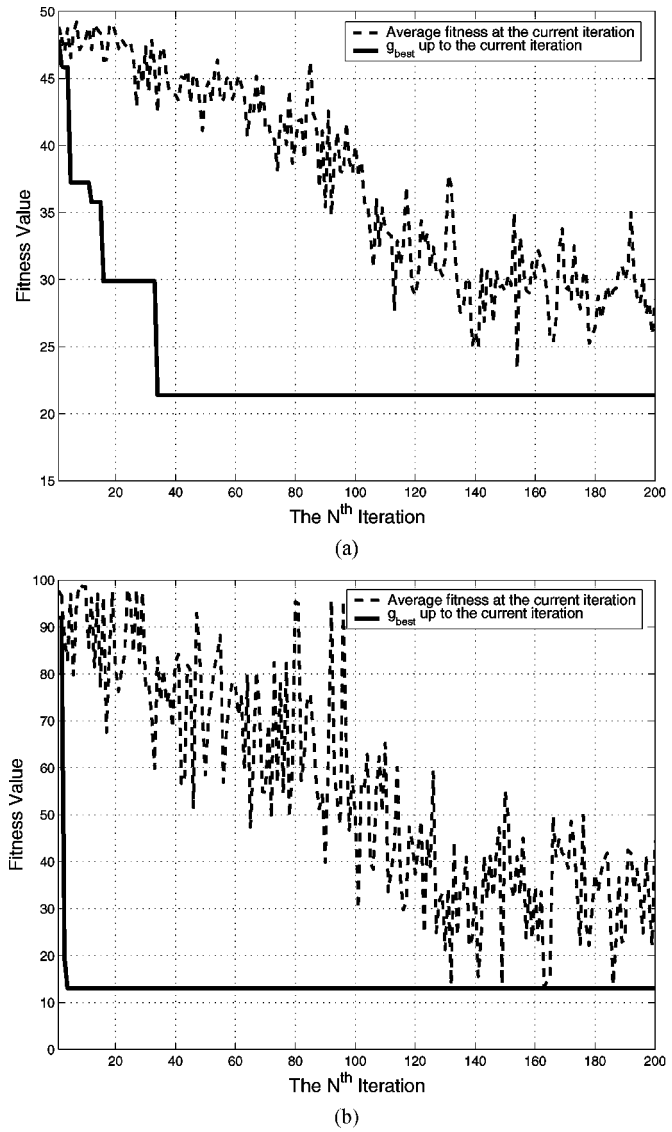

Fig. 4. Convergence results for rectangular patch antenna designs. The antennas are optimized (a) using fitness function in (7). (b) Using fitness function in (8).

where λ_0 is the free-space wavelength at the resonant frequency and t is the substrate thickness. Equations (9) and (10) predict that: 1) rectangular patches resonating at the same frequency have the same length; 2) the patch width is proportional to the bandwidth. These features are recovered by the optimization results, with the fitness functions only addressed on the antenna's S_{11}. It is also noticed that the width of antenna II is 44.0 mm, which exhibits the effectiveness of the optimizer even when the optimal design is located near the boundary of the solution space.

Fig. 4 shows the convergence results of the two optimizations. Two criteria are used in this paper to describe the convergence performance: the $g_{\rm best}$ *up to the current iteration* and the *average fitness at each iteration*. In optimization I, the best fitness value appears at the 34th iteration. The mean value of the oscillation in the average fitness value decreases and approaches $g_{\rm best}$ toward the end. Similar features are observed in Fig. 4(b), except for that the optimal design appears soon after the optimization starts (at the 5th iteration).

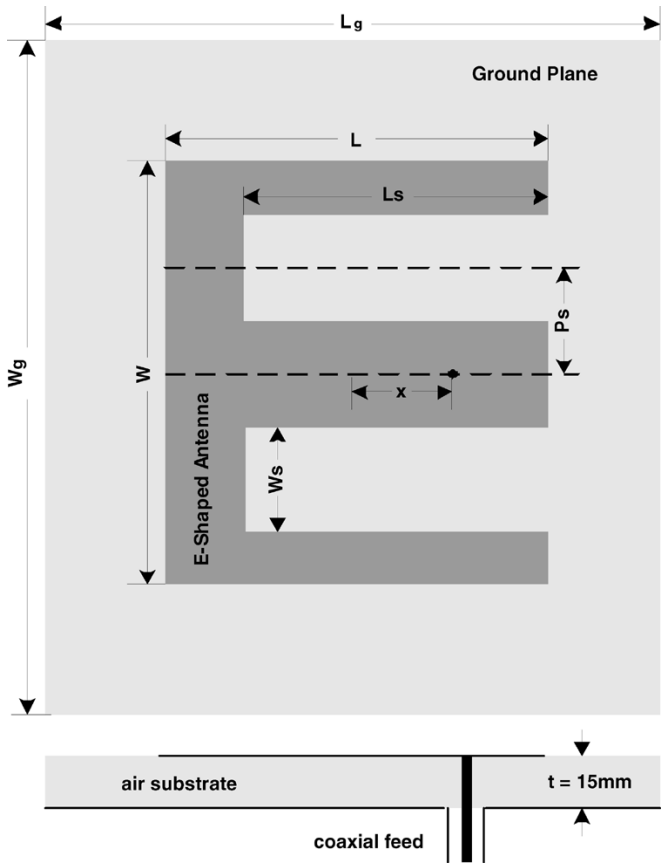

Fig. 5. Configuration of an E-shaped patch antenna. There are six geometrical parameters to be optimized by the parallel PSO/FDTD algorithm.

Using four parallel processors each, the two optimizations finish in 25 and 16 h, respectively. The time duration can be further reduced by applying the same number of processors as the particles, for instance, use 10 processors for the 10-particle swarm. Nevertheless, the optimization time has been greatly reduced by applying the RPC scheme. The particle positions and the number of actually simulated positions are investigated in both optimizations. In optimization I, 1872 positions (the possible maximum is 2000, other $2000 - 1872 = 128$ positions are out of the boundary) are encountered in the solution space, and all would be simulated by FDTD without applying RPC. The investigation shows that only 677 positions are *not-repeated positions* and actually simulated. In optimization II, only 357 positions are simulated among 1344 encountered ones. An optimization using the same swarm configuration is experimented without applying RPC scheme. The elongated, 49-h time duration validates the capability of the RPC scheme in reducing the computational time.

IV. Parallel PSO/FDTD Optimization for E-Shaped Patch Antenna Designs

Rectangular patch antenna extends its functionality by cutting slots in the patch to introduce multiple resonances. Recently a novel slotted antenna reported in [19] has become prevalent in wireless communication applications [20]. Two identical slots are cut on the same edge of a rectangular patch, which makes the antenna resemble a letter "E" and named E-shaped antenna

accordingly. The configuration of an E-shaped patch antenna is shown in Fig. 5. The geometrical parameters are also labeled in the figure. A coaxial feed is mounted in the central stub, which introduces two possible resonant lengths to generate different resonant frequencies. At the higher frequency, the current flows in the middle of the patch, which resembles a rectangular patch. At the lower frequency, the current flows around the slot and the resonant length is increased. By exploiting different coupling between the two resonances, the antenna exhibits either dual-frequency or wide-band performance.

Due to the complexity of the antenna topology, it is hard to quantitatively estimate the effect of each geometrical parameter to achieve the desired antenna performance. The parallel PSO/FDTD algorithm is applied in this section to accommodate this challenge. It is desired to optimize two E-shaped antennas with the performance of: 1) antenna I resonates at two frequencies of 1.8 GHz (for PCS applications) and 2.4 GHz (for bluetooth applications). 2) antenna II covers the entire frequency range from 1.8 to 2.4 GHz with acceptable return loss $S_{11} < -10$ dB.

A. Optimization Setup and Convergence

As shown in Fig. 5, the geometrical parameters to be optimized are: the patch length L, the patch width W, the slot length L_s, the slot width W_s, the slot position P_s, and the feed position x. The dimension of the solution space is six. The ground plane is fixed at 100 mm × 120 mm, and a 15-mm-thick air substrate is used to achieve the potential wide-band performance. In each optimization a 10-particle swarm is utilized. Due to the increased dimension of the solution space, the optimizations are performed by a greater maximum iteration of 1000. The geometrical parameters are optimized within (unit: mm)

$$\begin{aligned} &L \in (30, 96); \quad W \in (30, 96); \quad L_s \in (0, 96); \\ &W_s \in (0, 48); \quad P_s \in (0, 48); \quad x \in (-48, 48). \end{aligned} \tag{11}$$

To maintain the E-shaped structure, the following conditions must also hold as the additional geometrical restrictions

$$L_s < L; \quad \text{The slot can not cross the patch.} \tag{12}$$

$$P_s > \frac{W_s}{2}; \quad \text{The central stub must exist.} \tag{13}$$

$$P_s + \frac{W_s}{2} < \frac{W}{2}; \quad \text{The top and bottom stubs must exist.} \tag{14}$$

$$|x| < \frac{L}{2}; \quad \text{The feed can not go beyond the patch.} \tag{15}$$

Equations (11) – (15) completely defines the boundary of the solution space.

Two fitness functions are defined to evaluate the performances of the candidate designs. For antenna I, the worse return loss at the two desired frequencies is optimized using

$$f_1 = 50 + \max(S_{11,\,1.8\text{ GHz}}, S_{11,\,2.4\text{ GHz}}). \tag{16}$$

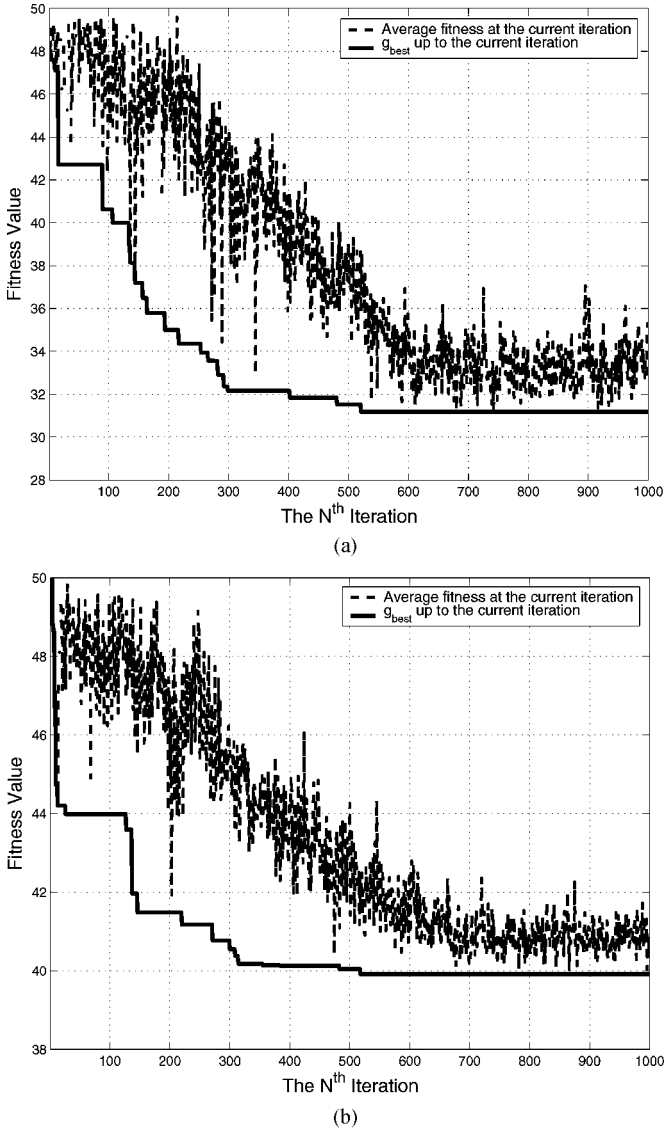

Fig. 6. Convergence results for E-shaped antenna designs. (a) The optimization of antenna I (dual-frequency antenna). (b) The optimization of antenna II (wide-band antenna).

For antenna II, the worst return loss in the entire frequency range from 1.8 to 2.4 GHz is optimized by

$$f_2 = 50 + \max(S_{11,\text{ from }1.8\text{ to }2.4\text{ GHz}}) \tag{17}$$

to achieve the wide-band feature. Compared to the rectangular patch antenna design, we use a different fitness function to obtain the desired bandwidth since the frequency region is specified. The fitness functions in (16) and (17) are inspired by the patch antenna optimizations using GA/MoM algorithm [12]; however, the FDTD algorithm takes advantage in getting broad frequency domain information. The S_{11} curve in the entire frequency domain is obtained via only one FDTD simulation.

Fig. 6(a) and (b) illustrates the convergence results of the two optimizations. Due to the complexity of the solution space, the best design is obtained after the 500th iteration in each optimization. The average fitness converges to the g_{best} toward the end of optimization. According to the record of the actual evaluated particle positions, the effectiveness of the RPC scheme is again

TABLE II
GEOMETRICAL PARAMETERS OF THE OPTIMIZED E-SHAPED PATCH ANTENNAS (UNIT: MILLIMETERS)

Design	L	W	L_s	W_s	P_s	x
Antenna I	54.0	46.0	47.0	20.0	12.0	14.0
Antenna II	52.0	82.0	48.0	20.0	12.0	13.0

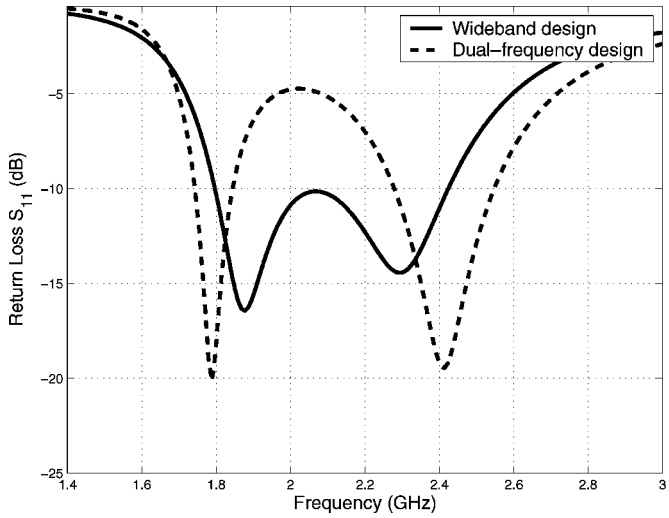

Fig. 7. Simulated return loss curves of the two optimized E-shaped patch antennas. The dual-frequency antenna operates at 1.8 and 2.4 GHz, and the wide-band antenna has a 30.5% $S_{11} < -10$ dB bandwidth that covers the desired frequency range.

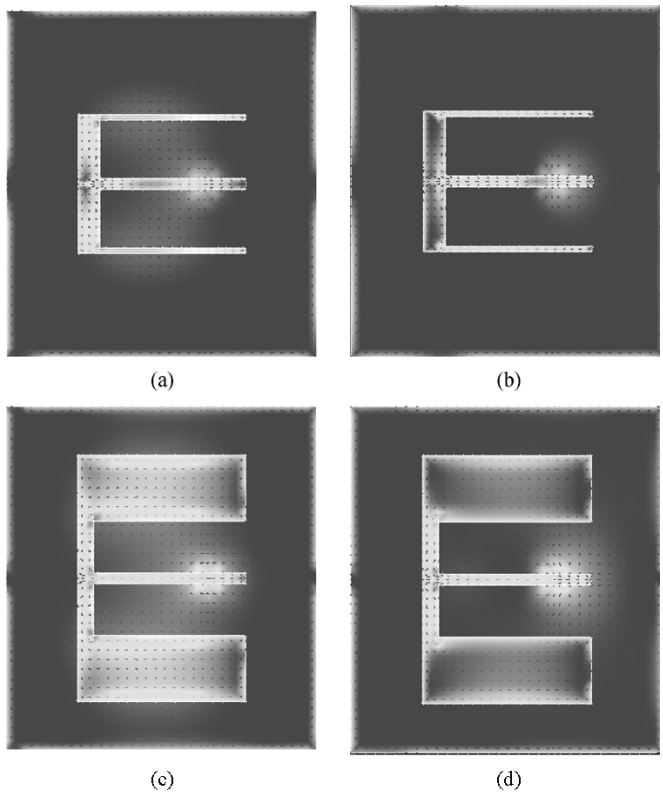

Fig. 8. Simulated current distributions of the two optimized E-shaped patch antennas. (a) Antenna I, at 1.8 GHz. (b) Antenna I, at 2.4 GHz. (c) Antenna II, at 1.85 GHz. (d) Antenna II, at 2.2 GHz.

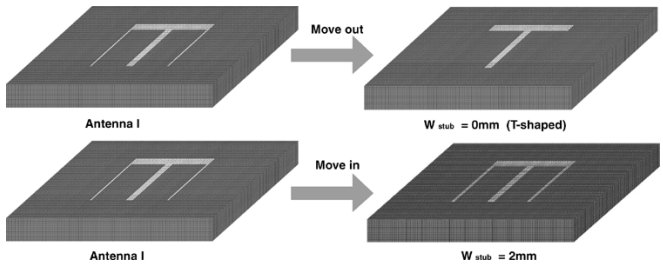

Fig. 9. Two alternative designs, a T-shaped antenna and an antenna with $W_{\text{stub}} = 2$ mm are developed from the optimized antenna I (dual-frequency antenna), by moving the particle position out of and into the solution space.

verified. In optimization I, 3150 FDTD simulations are executed among 6974 encountered positions. In optimization II, there are only 2160 *not-repeated positions* being simulated out of 6766 encountered positions.

B. Optimization Results

The optimized geometric parameters are listed in Table II. The simulated S_{11} curves are shown in Fig. 7. As expected, the parallel PSO/FDTD algorithm optimizes the S_{11} of antenna I at the two desired resonant frequencies and improves the relatively worse S_{11} value. The optimum design has S_{11} values of -18.5 and -19.4 dB at 1.8 and 2.4 GHz, respectively. The associated bandwidths are 110 MHz at 1.8 GHz (6.1%) and 270 MHz at 2.4 GHz (11.2%). On the other hand, with the worst S_{11} value in the desired frequency range being optimized, antenna II has a $S_{11} < -10$ dB bandwidth from 1.79 to 2.43 GHz (30.5%). It should be noted that even at the worst point, the return loss satisfies the $S_{11} < -10$ dB criterion ($S_{11} = -10.2$ dB at 2.04 GHz).

As shown in Table II, the two optimized antennas have approximately the same patch length, the same slot dimension, as well as the same feed position. The major difference between the two antennas lies in the patch widths. In fact the much wider patch width of antenna II reduces the Q value of each resonance. The coupling between the two resonances is hence increased to cover a broader frequency range. Fig. 8 shows the simulated current distributions. For both antennas, the current is concentrated in the central stub at the higher frequency, while distributed in top and bottom stubs at the lower frequency. Once again, the antenna operation mechanism predicted in [19] is recovered by the optimization results.

From Table II it is also noticed that the top and bottom stubs of antenna I are only 1-mm wide. Equation (14) shows that this design is located near the boundary of the solution space. Two alternative designs can be developed by changing the stub width by ± 1 mm, which effectively "move" the original design in and out of the solution space. This process is shown in Fig. 9. Specifically, the antenna with no top and bottom stubs is named as T-shaped antenna according to its topology.

The S_{11} curves of the three antennas with different stub widths are compared in Fig. 10. When the stub width is increased by 1 mm, the antenna shows 1-dB deteriorated return loss values at both 1.8 and 2.4 GHz. However, when the stubs are removed, the resonance at the lower frequency completely disappears without greatly affecting the resonance at the higher

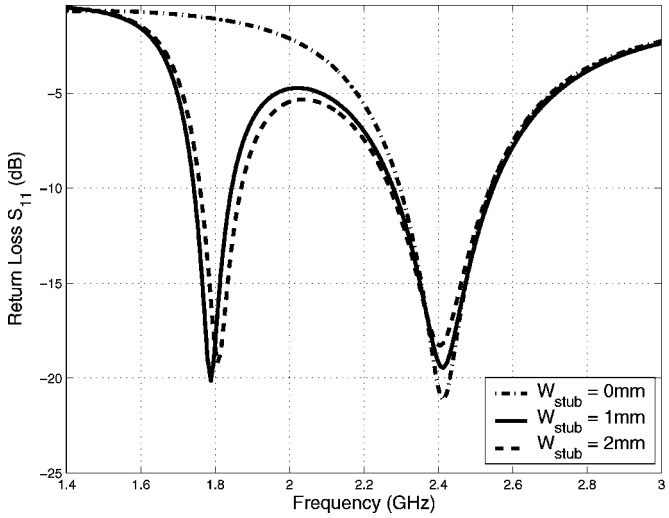

Fig. 10. Simulated S_{11} curves for the three antennas with $W_{\rm stub} = 0$ mm (T-shaped antenna), $W_{\rm stub} = 1$ mm (antenna I) and $W_{\rm stub} = 2$ mm.

frequency. The effect of changing stub widths emphasizes the importance to maintain the E-shape of the patch during the optimization. Moreover, the results in Fig. 10 convince us that, although the *invisible* boundary condition is used, the optimizer is able to achieve the best design located near the boundary of a complicated solution space.

C. Antenna Fabrications and Measurements

The optimized antennas are fabricated and measured in UCLA antenna lab to test the accuracy of the parallel PSO/FDTD algorithm in practical patch antenna designs. The photographs of the fabricated antenna prototypes are shown in Fig. 11. Fig. 12 plots the S_{11} curves measured by HP8510B network analyzer. The measured results agree well with the simulation results shown in Fig. 7, despite a slight frequency shift. The fabricated wide-band antenna exhibits a better return loss at the worst point in the band with a 2-dB improvement. The measured radiation patterns of the optimized antennas are plotted in Figs. 13 and 14. As described in [19], the E-shaped antenna has similar patterns to a rectangular patch antenna but with relatively high cross polarizations in H-plane. The radiation patterns of the wide-band antenna are measured at 1.85 and 2.2 GHz, where the best S_{11} values are observed. Both antennas have broadside directivities greater than 7 dBi, which confirms their potential applications in wireless communications.

V. Conclusion

In this paper, a novel evolutionary optimization algorithm is applied in patch antenna designs. The optimization kernel was constructed using PSO and FDTD was integrated into the optimizer for fitness evaluations. The utilization of *invisible* boundary condition and RPC scheme reduces the computational burden imposed by the full-wave analysis. The optimization process was implemented on parallel clusters to further reduce the computational time.

The parallel PSO/FDTD algorithm was tested by designing rectangular patch antennas. The design criterion was to obtain satisfactory antenna return loss and bandwidth. The procedure

(a)

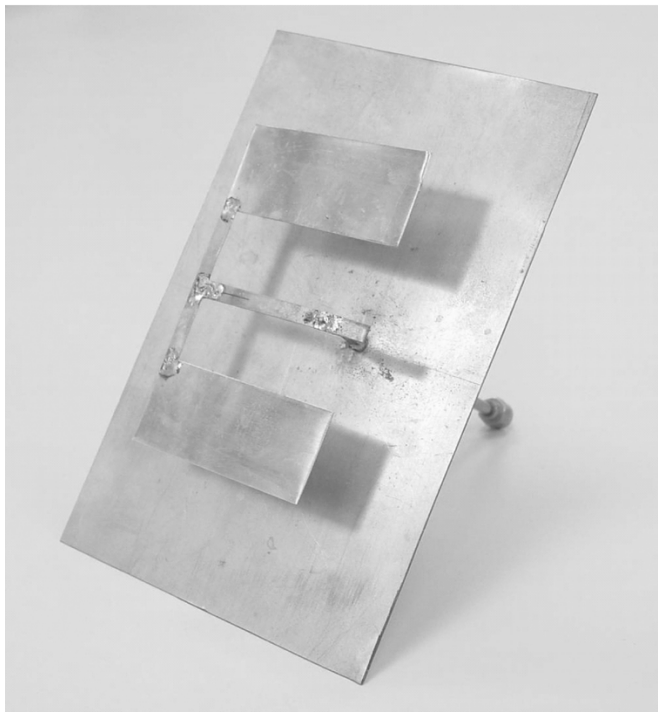

(b)

Fig. 11. Photographs of the fabricated antenna prototypes. (a) Antenna I (dual-frequency antenna). (b) Antenna II (wide-band antenna).

and the results of the optimizations show that the parallel PSO/FDTD optimizer is able to achieve the optimum design for specified antenna performance in an effective manner. Subsequently the algorithm was utilized to design more complicated E-shaped patch antennas. Using different fitness functions, a dual-frequency antenna and a wide-band antenna were designed. The dual-frequency antenna operates at 1.8 and

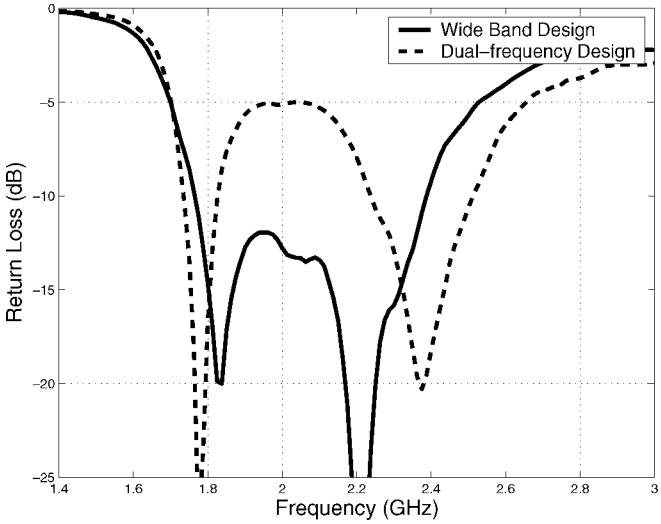

Fig. 12. Measured return loss curves of the two fabricated E-shaped patch antennas. The measurement results agree well with the simulation results in Fig. 7.

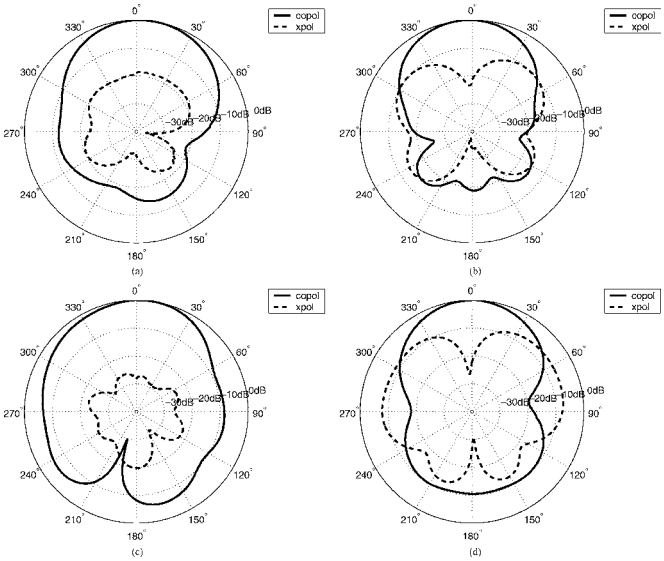

Fig. 13. Measured radiation patterns of the optimized antenna I (dual-frequency antenna). (a) E-plane, at 1.8 GHz. (b) H-plane, at 1.8 GHz. (c) E-plane, at 2.4 GHz. (d) H-plane, at 2.4 GHz.

2.4 GHz with $S_{11} < -18$ dB at both frequencies. The wide-band antenna has a $S_{11} < -10$ dB bandwidth from 1.79 to 2.43 GHz (30.5%). The analysis of the optimized antennas provides further understanding of the antenna operation mechanism and the performance of the parallel PSO/FDTD algorithm in practical patch antenna designs. The measurement results of the optimized E-shaped antennas agree well with the simulation results. The accuracy and the robustness of the parallel PSO/FDTD algorithm validate its potential application in the antenna designs for wireless communications.

REFERENCES

[1] S. Weigand, G. H. Huff, K. H. Pan, and J. T. Bernhard, "Analysis and design of single-layer rectangular u-slot microstrip patch antennas," *IEEE Trans. Antennas Propag.*, vol. 51, no. 3, pp. 457–468, Mar. 2003.

[2] J. Robinson and Y. Rahmat-Samii, "Particle swarm optimization in electromagnetics," *IEEE Trans. Antennas Propag.*, vol. 52, no. 2, pp. 397–407, Feb. 2004.

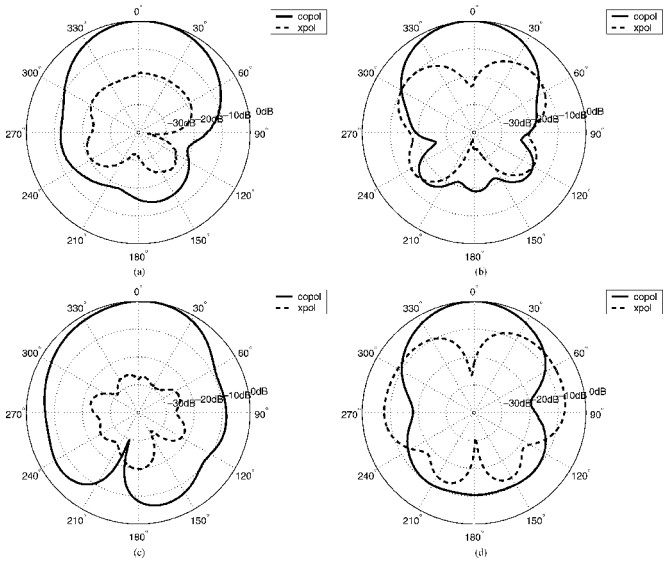

Fig. 14. Measured radiation patterns of the optimized antenna II (wide-band antenna). (a) E-plane, at 1.85 GHz. (b) H-plane, at 1.85 GHz. (c) E-plane, at 2.2 GHz. (d) H-plane, at 2.2 GHz.

[3] J. Kennedy and R. Eberhart, "Particle swarm optimization," in *Proc. 1995 Int. Conf. Neural Networks*, vol. IV, Perth, Australia, 1995, pp. 1942–1948.

[4] Y. Rahmat-Samii and E. Michielssen, Eds., *Electromagnetic Optimization by Genetic Algorithms*. New York: Wiley, 1999.

[5] D. Gies and Y. Rahmat-Samii, "Particle swarm optimization for reconfigurable phase-differentiated array design," *Microw. Opt. Technol. Lett.*, vol. 38, no. 3, pp. 172–175, Aug. 2003.

[6] D. Boeringer and D. Werner, "Particle swarm optimization versus genetic algorithms for phased array synthesis," *IEEE Trans. Antennas Propag.*, vol. 52, no. 3, pp. 771–779, Mar. 2004.

[7] D. Gies and Y. Rahmat-Samii, "Vector evaluated particle swarm optimization (VEPSO): Optimization of a radiometer array antenna," in *2004 IEEE Antennas Propagat. Soc. Int. Symp. Dig.*, vol. 3, Jun. 2004, pp. 2297–2300.

[8] J. Robinson, S. Sinton, and Y. Rahmat-Samii, "Particle swarm, genetic algorithm, and their hybrids: Optimization of a profiled corrugated horn antenna," in *2002 IEEE Antennas Propagat. Soc. Int. Symp. Dig.*, vol. 1, Jun. 2002, pp. 314–317.

[9] D. Gies and Y. Rahmat-Samii, "Particle swarm optimization (PSO) for reflector antenna shaping," in *2004 IEEE Antennas Propagat. Soc. Int. Symp. Dig.*, vol. 3, Jun. 2004, pp. 2289–2293.

[10] C. Coello, G. Pulido, and M. Lechuga, "Handling multiple objectives with particle swarm optimization," *IEEE Trans. Evol. Comput.*, vol. 8, no. 3, pp. 256–279, Jun. 2004.

[11] D. Gies, "Particle swarm optimization: Applications in electromagnetic design," M. S., Univ. California, Los Angeles, 2004.

[12] J. Johnson and Y. Rahmat-Samii, "Genetic algorithms and method of moments (GA/MOM) for the design of integrated antennas," *IEEE Trans. Antennas Propag.*, vol. 47, no. 10, pp. 1606–1614, Oct. 1999.

[13] F. Villegas, T. Cwik, Y. Rahmat-Samii, and M. Manteghi, "A parallel electromagnetic genetic-algorithm optimization (EGO) application for patch antenna design," *IEEE Trans. Antennas Propag.*, vol. 52, no. 9, pp. 2424–2435, Sep. 2004.

[14] H. Lebbar, M. Himdi, and J. Daniel, "Analysis and optimization of reduced size printed monopole," in *1993 IEEE Antennas Propag. Soc. Int. Symp. Dig.*, vol. 3, Jun. 1993, pp. 1858–1861.

[15] M. Himdi and J. Daniel, "Synthesis of slot coupled loaded patch antennas using a genetic algorithm through various examples," in *1997 IEEE Antennas Propag. Soc. Int. Symp. Dig.*, vol. 3, Jul. 1997, pp. 1700–1703.

[16] Y. Shi and R. Eberhart, "A modified particle swarm optimizer," in *Proc. IEEE Int. Conf. Evolutionary Computation*, 1998, pp. 69–73.

[17] D. Velduizen, J. Zydallis, and G. Lamount, "Considerations in engineering parallel multiobjective evolutionary optimizations," *IEEE Trans. Evol. Comput.*, vol. 7, no. 2, pp. 144–173, Apr. 2002.

[18] W. L. Stutzman and G. A. Thiele, *Antenna Theory and Design*, 2nd ed. New York: Wiley, 1998.

[19] F. Yang, X. X. Zhang, X. Ye, and Y. Rahmat-Samii, "Wide-band E-shaped patch antennas for wireless communications," *IEEE Trans. Antennas Propag.*, vol. 49, no. 7, pp. 1094–1100, Jul. 2001.

[20] Y. Ge, K. P. Esselle, and T. S. Bird, "E-shaped patch antennas for high-speed wireless networks," *IEEE Trans. Antennas Propag.*, vol. 52, no. 12, pp. 3213–3219, Dec. 2004.

Nanbo Jin (S'03) received the B.S. degree from Tsinghua University, Beijing, China, in 2003, and the M.S. degree from the University of California, Los Angeles (UCLA), in 2005, all in electrical engineering.

He is currently working toward the Ph.D. degree at UCLA in electrical engineering. From 2001 to 2003, he was a Research Assistant with the State Key Laboratory of Microwave and Digital Communications, Tsinghua University. Since August 2003, he has been working as a Graduate Research Assistant in the UCLA Antenna Laboratory. His research interests are particle swarm optimization technique, microstrip and reconfigurable antenna design, and periodic structures in electromagnetic applications.

Yahya Rahmat-Samii (S'73–M'75–SM'79–F'85) received the M.S. and Ph.D. degrees in electrical engineering from the University of Illinois, Urbana-Champaign.

He was a Guest Professor with the Technical University of Denmark (TUD) during summer 1986. He was a Senior Research Scientist at NASA's Jet Propulsion Laboratory, California Institute of Technology, Pasadena, before joining the University of California, Los Angeles (UCLA) in 1989. Currently, he is a Distinguished Professor and the Chairman of the Electrical Engineering Department, UCLA. He has also been a Consultant to many aerospace companies. He has been Editor and Guest Editor of many technical journals and book publication entities. He has authored and coauthored more than 660 technical journal articles and conference papers and has written 20 book chapters. He is the coauthor of *Impedance Boundary Conditions in Electromagnetics* (Washington, DC: Taylor & Francis, 1995) and *Electromagnetic Optimization by Genetic Algorithms* (New York: Wiley, 1999). He is also the holder of several patents. He has had pioneering research contributions in diverse areas of electromagnetics, antennas, measurement and diagnostics techniques, numerical and asymptotic methods, satellite and personal communications, human/antenna interactions, frequency selective surfaces, electromagnetic band-gap structures and the applications of the genetic algorithms. On several occasions, his work has made the cover of many magazines and has been featured on several television newscasts.

Dr. Rahmat-Samii is a Member of Sigma Xi, Eta Kappa Nu, Commissions A, B, J, and K of the United States National Committee for the International Union for Radio Science (USNC/URSI), Antennas Measurement Techniques Association (AMTA), and the Electromagnetics Academy. He was elected as a Fellow of the Institute of Advances in Engineering (IAE) in 1986. Since 1987, he has been designated every three years as one of the Academy of Science's Research Council Representatives to the URSI General Assemblies held in various parts of the world. In 2001, he was elected as the Foreign Member of the Royal Academy of Belgium for Science and the Arts. He was also a member of UCLA's Graduate council for a period of three years. For his contributions, he has received numerous NASA and JPL Certificates of Recognition. In 1984, he received the coveted Henry Booker Award of the URSI which is given triennially to the Most Outstanding Young Radio Scientist in North America. In 1992 and 1995, he was the recipient of the Best Application Paper Prize Award (Wheeler Award) for papers published in the 1991 and 1994 IEEE ANTENNAS AND PROPAGATION. In 1999, he was the recipient of the University of Illinois ECE Distinguished Alumni Award. In 2000, he was the recipient of IEEE Third Millennium Medal and AMTA Distinguished Achievement Award. In 2001, he was the recipient of the Honorary Doctorate in physics from the University of Santiago de Compostela, Spain. In 2002, he received the Technical Excellence Award from JPL. He is the winner of the 2005 URSI Booker Gold Medal to be presented at the URSI General Assembly. He was also a Member of the Strategic Planning and Review Committee (SPARC) of the IEEE. He was the IEEE AP-S Los Angeles Chapter Chairman (1987–1989) and his chapter won the Best Chapter Awards in two consecutive years. He was the elected 1995 President and 1994 Vice-President of the IEEE Antennas and Propagation Society. He was one of the Directors and Vice President of the Antennas Measurement Techniques Association (AMTA) for three years. He was appointed an IEEE Antennas and Propagation Society Distinguished Lecturer and presented lectures internationally. He is listed in *Who's Who in America*, *Who's Who in Frontiers of Science and Technology*, and *Who's Who in Engineering*. He is the designer of the IEEE Antennas and Propagation Society logo that is displayed on all IEEE ANTENNAS AND PROPAGATION publications.